JOURNAL OF SPACECRAFT AND ROCKETS
Vol. 37, No. 5, September–October 2000

Repeat Orbit Characteristics and Maneuver Strategy for a Synthetic Aperture Radar Satellite

H. J. Rim,* B. E. Schutz,† C. E. Webb,‡ and P. Demarest‡
University of Texas at Austin, Austin, Texas 78712
and
A. Herman§
Spectrum Astro, Inc., Gilbert, Arizona 85234

A newly proposed synthetic aperture radar Earth-imaging mission, LightSAR, requires the orbit to be maintained within a 125-m-radius tube centered on a reference orbit over the lifetime of the satellite. A reference orbit was defined that repeats every eight days and has a ground-track closure of about 8 cm and a radial closure of about 16 m at the end of the repeat interval. Major perturbing forces were investigated to determine the length of time before the perturbed orbit violated the tube constraint. The forces examined include Earth gravity (including tides), luni–solar gravity, atmospheric drag, and radiation pressure. Of these perturbations, atmospheric drag and luni–solar gravity were the dominant perturbations leading to violation of the tube constraint. A maneuver strategy was developed to meet the stringent orbit maintenance requirement of staying within 125 m of the reference orbit. A series of maneuvers directed in the tangential and normal directions and applied at fixed time intervals was able to maintain the satellite position within the tube for eight days. The additional application of a maneuver in the radial direction allows the maneuver strategy developed to be effective for up to four repeat cycles, nearly 32 days. In all, 31 maneuvers with a total ΔV of 910.659 mm/s were required in the assumed dynamic environment to maintain the spacecraft within 125 m of the reference orbit during this interval.

Nomenclature

A	=	satellite cross-sectional area, m^2
a	=	semimajor axis, m
C_d	=	atmospheric drag coefficient
C_r	=	reflectivity coefficient
D	=	distance from reference orbit in radial/cross-track plane, m
$D_{\max}$	=	maximum distance from reference orbit in radial/cross-track plane, m
D^*	=	penalty function trigger, effective tube radius, m
e	=	eccentricity
$F_{10.7}$	=	solar flux at 10.7-cm wavelength
f	=	subscript denoting value at final time
G	=	performance index
i	=	inclination, deg
K_p	=	geomagnetic index
k	=	iteration number
M	=	mean anomaly, deg
m	=	satellite mass, kg
R–C	=	radial and cross track
t_b	=	timing bias in orbit comparison, s
t_f	=	final time of repeat-cycle interval, s
t_m	=	interval between maneuvers, s
t_0	=	initial time of repeat-cycle interval, s
u	=	argument of latitude, °
W	=	penalty function weight
ΔV	=	change in velocity, mm/s
ΔV_N	=	normal component of ΔV, mm/s
ΔV_{N_0}	=	weight for normal component of ΔV
ΔV_R	=	radial component of ΔV, mm/s
ΔV_T	=	tangential component of ΔV, mm/s
ΔV_{T_0}	=	weight for tangential component of ΔV
λ	=	geodetic longitude, °
ϕ	=	geodetic latitude, °
Ω	=	right ascension of ascending node, deg
ω	=	argument of perigee, deg
0	=	subscript denoting value at initial time

Received 8 May 1998; accepted for publication 10 July 2000.

*Research Associate, Center for Space Research.
†Professor and Associate Director, Center for Space Research.
‡Research Assistant, Center for Space Research.
§Principal Mission Analyst.

Introduction

THE LightSAR satellite has been proposed as a part of NASA's Earth Sciences Enterprise program to provide high-resolution images on a nearly continuous basis, to map changes in land cover, to generate topographic maps, and to provide long-term mapping of natural hazards using synthetic aperture radar (SAR) measurements. The SAR interferometric imaging requirements demand that the LightSAR orbit be maintained within a 125-m-radius tube centered on a reference orbit. Such unprecedented orbit maintenance requirements pose new challenges in the development of a satisfactory maneuver strategy. Proceeding from mission design work conducted by Lim and Schutz[1] for ICESat and the TOPEX/Poseidon orbit maintenance plan developed by Bhat et al.,[2] this paper addresses the following aspects of the problem: 1) defining a reference orbit with satisfactory closure at the end of the repeat interval, 2) investigating the major perturbing forces that produce deviations from the reference orbit, and 3) investigating and developing a maneuver strategy to maintain the LightSAR orbit within the required tube.

The mission requirements for this study prescribe that the orbit plane have an inclination near 81 deg. Three orbits were found that meet the repeat and inclination requirements. For the purposes of this study a reference orbit that repeats every eight days after 117 revolutions at an inclination of 81.8 deg was selected.

Perturbing forces were investigated to determine whether, and how quickly, they caused the satellite to violate the tube boundary. The forces examined include Earth gravity (including tides), luni–solar gravity, atmospheric drag, and radiation pressure.

The maneuver strategy developed under this study attempts to find the smallest maneuver that keeps the satellite within the tube for a fixed interval of time. Maneuvers were calculated with components in two directions, typically, the tangential and normal.

Reference Orbit

For the LightSAR mission, the tube constraint on the motion of the spacecraft must be applied relative to a specified reference orbit. Defined in an Earth-fixed coordinate system, the reference orbit is

Table 1 Reference orbit mean elements

Orbit element	Value
a, m	7,031,474.54700
$e \times 0.001$	1.1906698
i, deg	81.8
ω, deg	90.0

circumscribed by a 125-m-radius tube within which the satellite must remain at all times. The presence of both gravitational and nongravitational perturbations causes the actual orbit to deviate from the reference, eventually forcing the spacecraft out of this tube. With an appropriate strategy, propulsive maneuvers can be employed to compensate for these perturbing forces so that the tube constraint will be satisfied.

To minimize the magnitudes of the maneuvers required to counter these perturbations, the reference orbit should incorporate as many of the anticipated disturbing forces as practical. Ideally, a periodic orbit that returns the satellite to its initial conditions after the desired eight-day repeat interval would be found to exist in the presence of a complete force model. However, the influence of nongravitational forces, notably the nonconservative forces associated with atmospheric drag and radiation pressure, precludes the determination of such a periodic orbit. Additionally, the gravitational effects of the sun and the moon, which vary with time and have periods exceeding the eight-day repeat interval, hinder the establishment of an exact repeat orbit. As a result, the selected reference orbit reflects the geopotential only, modeled using JGM-3 (Ref. 3), through degree and order 70 (denoted as 70×70).

To determine a suitable reference orbit, the method developed by Lim and Schutz[1] has been employed. Lim and Schutz[1] indicate that for altitudes near that of the LightSAR spacecraft, the frozen eccentricity does not depend significantly on the zonal harmonics beyond degree 31. Consequently, the mean semimajor axis and the corresponding frozen eccentricity that yield the desired repeating orbit characteristics are computed in a 31×0 geopotential field. These values, along with the mean inclination and argument of perigee, are shown in Table 1. The corresponding altitude is approximately 650 km.

Osculating orbit elements were obtained by applying short-period terms through the first order, using Kaula's theory.[4] When the equations of motion are numerically integrated in the 31×0 geopotential model, the initial semimajor axis and eccentricity were iterated to close the ground track, thus achieving two-dimensional repeatability in the orbit. When the resulting trajectory is adopted as the truth orbit, an estimation of all six of the initial osculating elements was then made in the presence of the 70×70 geopotential model. Final closure of the ground track was obtained through additional iteration of the semimajor axis and eccentricity. In both instances, their values were updated using a Newton–Raphson algorithm:

$$\begin{bmatrix} a_0 \\ e_0 \end{bmatrix}_{k+1} = \begin{bmatrix} a_0 \\ e_0 \end{bmatrix}_k - \begin{bmatrix} \dfrac{\partial u_f}{\partial a_0} & \dfrac{\partial u_f}{\partial e_0} \\ \dfrac{\partial \omega_f}{\partial a_0} & \dfrac{\partial \omega_f}{\partial e_0} \end{bmatrix}^{-1} \begin{bmatrix} u_f - u_0 \\ \omega_f - \omega_0 \end{bmatrix} \quad (1)$$

The partial derivatives in Eq. (1) were numerically approximated. The initial osculating state corresponded to a mean position in the orbit at the ascending node. The final time of the trajectory t_f, which defines the ground-track repeat interval, was adjusted during the closure process so that the satellite returned to its initial geodetic latitude and longitude within an acceptable tolerance. Once a satisfactory ground-track closure was achieved, the radius at the beginning and end of the repeat cycle was examined to determine the repeatability of the orbit in three dimensions. Table 2 summarizes the initial and final osculating states for the 70×70 reference orbit.

In addition, Table 2 characterizes the repeatability of the reference orbit in the Earth-fixed system. Whereas the offsets at t_f in geodetic latitude and longitude correspond to only 7.5 cm in ground-track misclosure, there remains a notably larger radial offset of 16 m. However, because its magnitude is small enough relative to the 125-m tube constraint, the three-dimensional repeatability of the reference orbit was considered to be acceptable for this analysis.

Table 2 Reference orbit osculating initial and final conditions, epoch: 1 January 2000 0:00:00

Parameter	Initial	Final	Difference
Time, s	0.000000	687,394.7543204	687,394.7543204
a, m	7,040,775.066	7,040,775.022	−0.044
$e \times 0.001$	1.30422184	1.29243432	−0.01178752
i, deg	81.80645491	81.80645503	0.00000012
Ω, deg	359.99922683	351.98581425	−8.01341258
ω, deg	66.40858554	66.29133853	−0.11724701
M, deg	293.71483206	293.83071969	0.11588764
Radius, m	7,037,091.958	7,037,108.250	16.292
ϕ, °	−0.01336699	−0.01336763	−0.00000064
λ, °	−0.00269785	−0.00269763	0.00000022

Effects of Major Forces on the LightSAR Orbit

Major forces acting on the LightSAR spacecraft were considered individually to determine the effect of each perturbation on the LightSAR orbit. Because the LightSAR orbit must be maintained within the control tube, it is desirable to quantify the deviation from the reference orbit resulting from each of the major forces. Those forces considered in this study were Earth gravity, luni–solar gravity, atmospheric drag, and solar radiation pressure. In all cases, the perturbed orbits start from the same initial conditions of the reference orbit tabulated in Table 2. The University of Texas precision orbit software, UTOPIA, was used to propagate orbits for analysis. The deviations of the perturbed orbit from the reference orbit were measured in the R–C plane, defined by the satellite radius and orbit normal vectors. Note that the along-track deviation simply translates into a timing bias t_b, and even large along-track effects do not violate the tube constraint. The along-track deviation was removed in the orbit comparison in the R–C plane for this section, by comparing an orbit point at t for the reference orbit and a corresponding orbit point at $t - t_b$ for the perturbed orbit.

Earth Gravity

The reference orbit in the preceding section was defined based on the JGM-3 geopotential model up to degree and order 70. To evaluate the effect of geopotential model error on the LightSAR orbit, two orbits using different geopotential models with different degree and order truncations were compared. The EGM-96 model[5] up to degree and order 99 was used with the reference orbit initial conditions, and the resulting orbit was compared to the JGM-3 70×70 reference orbit. The differences in the R–C plane were less than 5 m over the repeat cycle. Although JGM-3 and EGM-96 are not completely independent, this result does suggest that errors in the gravity field will not be a significant contributor to any violation of the tube constraint.

Solid Earth Tides

Because the Earth is an elastic body to a certain extent, its mass distribution and shape will be changed under the gravitational attraction of the major perturbing bodies, especially the sun and the moon. This perturbation will vary from repeat cycle to repeat cycle. The effect of the solid Earth tides on the radial component of the LightSAR orbit over one repeat cycle was less than 20 cm, whereas the effect on the cross-track component reached more than 50 m at the end of eight days. For the cycle investigated, the overall effect of solid Earth tides did not violate the tube constraint.

Ocean Tides

The effect of the ocean tide perturbations, also induced by the sun and the moon, on the LightSAR orbit was an order of magnitude smaller than the solid Earth tidal effect. Using the Center for Space Research TOPEX/Poseidon Ocean Tides model[6] to generate the perturbations, the effects were about 1 m in the radial component and 5 m in the cross-track component at the end of the repeat cycle. These effects clearly do not violate the tube constraint.

Luni–Solar Gravity

The luni–solar gravity perturbations will introduce variations with significant amplitude and periods of 14 days (fortnightly) and 183 days (semiannually), as well as long-period (18.6 years) and secular effects on the node location. Because these periods are longer than the repeat cycle period, the luni–solar effects will change from repeat cycle to repeat cycle. Figure 1 shows an example of the effect of the luni–solar perturbations over an eight-day period after the epoch of the reference orbit. Note that the effect is mainly in the cross-track component, and the tube requirement is violated after about 3.9 days. Figure 2 shows the effects of the luni–solar perturbations on the LightSAR orbit inclination and longitude of the ascending node in the geocentric nonrotating J2000.0 system over a one-year period. The secular change in the node due to the luni–solar effects is evident. The inclination and node variations are the primary contributors to the cross-track component differences with the reference orbit. A 1-arc-s change in the inclination or in the node results in about 34-m deviation from the reference orbit in the cross-track component.

Atmospheric Drag

The orbit decay associated with drag necessitates the orbit adjustments required to maintain the repeat cycle. Figure 3 shows the effect of drag over the eight-day repeat cycle. The DTM model[7] with high solar flux conditions ($F_{10.7} = 200.0$ and $K_p = 2.0$) was used with $C_d A/m = 0.0293$ m^2/kg. The tube constraint was violated after only 0.88 day.

Radiation Pressure

Figure 4 shows the effect of solar radiation pressure on the LightSAR orbit over one repeat cycle. The effect was mainly in the radial component, and the tube requirement was not violated by the end of the repeat cycle. A constant area model of 33.7 m^2 with a reflectivity of 0.3 was used. Note that the solar radiation pressure effect is seasonal, and Fig. 4 shows the maximum effect because the distance between the sun and the satellite was the shortest over the investigated period. Also, note that the LightSAR orbit was in Earth shadow about 25% time during this one repeat cycle.

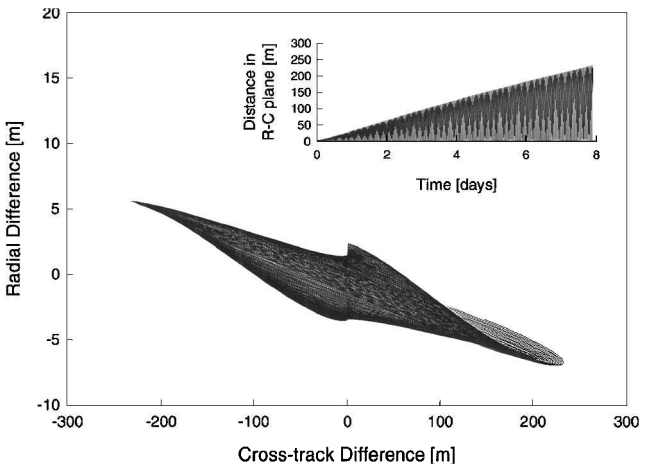

Fig. 1 Effect of luni–solar perturbations.

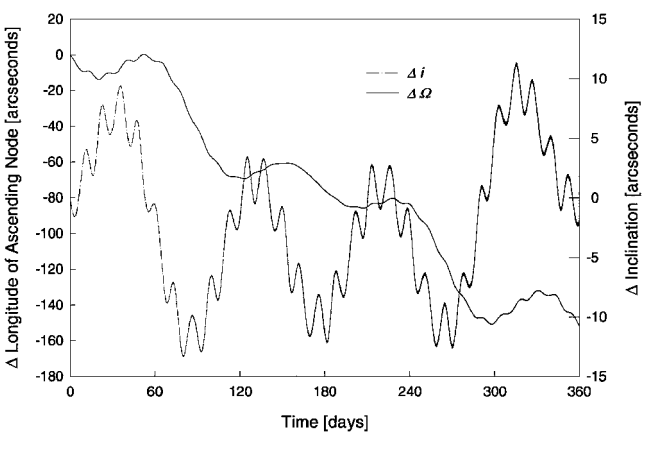

Fig. 2 Long-term effect of luni–solar perturbations.

Table 3 Effect of major forces on the LightSAR orbit over one repeat cycle

Perturbation	Maximum deviation from reference orbit, m: Radial	Cross track	Distance in R–C plane	Time for tube violation, day
Atmospheric drag	386.7	10,253.6	10,255.4	0.88
Sun and moon gravity	7.0	232.4	232.5	3.94
Radiation pressure	101.0	28.4	103.8	——
Solid Earth tides	0.2	53.1	53.1	——
Ocean tides	1.1	5.1	5.2	——

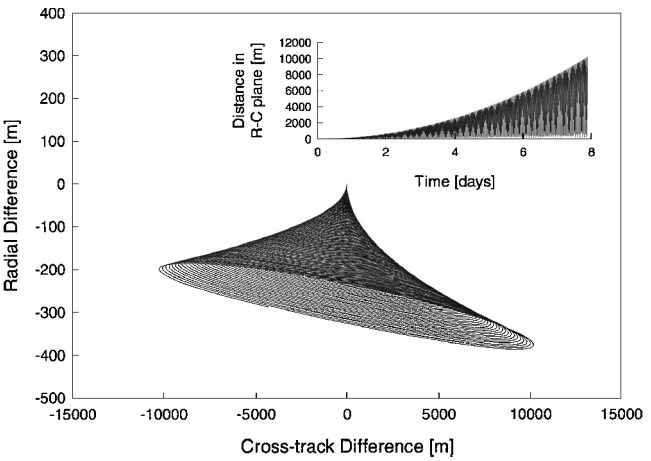

Fig. 3 Effect of atmospheric drag.

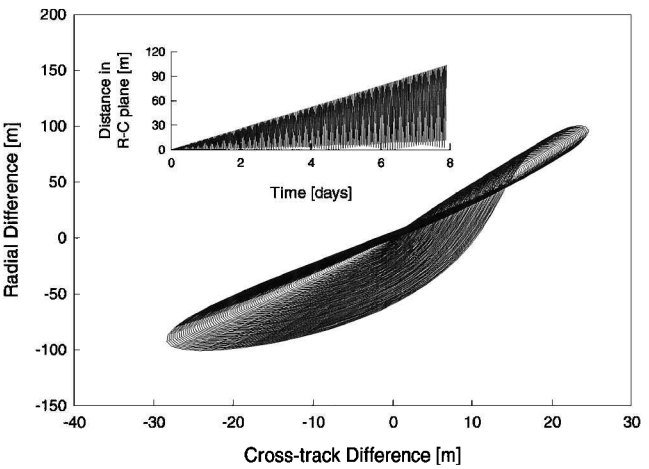

Fig. 4 Effect of solar radiation pressure.

The effects of Earth radiation pressure, which consists of Earth albedo and emissivity, were less than 10% of the total solar radiation pressure. Specific cases were not computed because the solar radiation component dominates the overall radiation pressure perturbation.

Maneuver Strategy

Table 3 summarizes the effects of the considered perturbing forces on the LightSAR orbit over one repeat cycle in relation to the tube constraint. From the analysis of the perturbations, it is seen that the actual orbit of the satellite will quickly violate the 125-m-tube boundary for the assumed conditions. To keep the satellite within the tube during its operational lifetime, a series of orbital maneuvers needs to be applied. Any maneuver strategy developed must maintain the orbit within the tube and do so in an efficient manner. This

section presents an investigation of one possible maneuver strategy and comments on its effectiveness and efficiency.

Maintaining the satellite orbit within a 125-m-radius tube is a much stricter requirement than that imposed on other exact repeat orbits such as TOPEX and GEOSAT. These satellites required maintenance of their ground tracks to within 1000 m of a reference at the equator. No requirement was made on the repeatability or closure of the radial component of the orbit. Because of this, both TOPEX[2] and GEOSAT[8] used a maneuver strategy based on the decay of the mean orbital elements of the satellite and used widely spaced tangential maneuvers to maintain the exact repeat of the ground track. This type of maneuver strategy is ineffective for maintaining a tube orbit for long periods of time.[9]

Atmospheric drag is the dominant perturbation on the satellite orbit, causing a predominantly radial deviation from the reference orbit. Luni–solar gravity is also a significant perturbation, causing a cross-track deviation from the reference. Development of a comprehensive maneuver strategy requires addressing both of these effects.

Fixed Interval Targeting

A maneuver strategy has been developed based on applying maneuvers with ΔV components in the tangential and normal directions at fixed intervals of time. The magnitudes of the ΔV components, ΔV_T and ΔV_N, were computed to minimize the following performance index:

$$G_1(\Delta V_T, \Delta V_N; t_m) = \sqrt{\left[\left(\Delta V_T / \Delta V_{T_0}\right)^2 + \left(\Delta V_N / \Delta V_{N_0}\right)^2\right]} + \max\left[0, \left(D_{\max} - D^*\right)/W\right] \quad (2)$$

This performance index combines the magnitude of the ΔV, which we want to minimize, with a penalty function that is used to exclude solutions where the satellite violates the tube constraint. The value of G_1 was calculated after propagating the orbit forward in time from the application of one maneuver to the next, over the predetermined maneuver interval, t_m. The parameters ΔV_{T_0}, ΔV_{N_0}, D^*, and W were preselected and held constant.

The performance index was minimized in the following manner. At a given epoch, an initial guess for the ΔV was applied, and the orbit was propagated forward in time, through one maneuver interval. From the propagated arc, the maximum deviation from the reference orbit in the R–C plane, $D_{\max}$, was computed, and the performance index evaluated. The gradient of G_1 was calculated to yield the initial search direction. A new ΔV was calculated and added to the original initial state. The orbit was again propagated forward, and G_1 was recalculated. This was repeated until a minimum of G_1 was found in the search direction.

A new search direction was chosen using the Davidon–Fletcher–Powell method (see Ref. 10). The minimum was found in this search direction, with a new arc integrated for each new ΔV. This was repeated until convergence at the minimum of the performance index was reached. Convergence was defined as a less than 1% change in the performance index. All orbits were simulated with UTOPIA, and the required partial derivatives were calculated numerically using forward differences. The state of the satellite at the end of the maneuver interval was then used as the initial state for planning the next maneuver.

In this study, t_m was chosen so that the maneuvers would always be applied near the equator. This approach was adopted to prevent the normal component of the ΔV from inducing a precession of the eccentricity vector. Additionally, t_m was selected so that the location of the maneuvers alternated between the ascending and descending nodes. This consideration was made to keep the eccentricity vector bounded and thus maintain the frozen characteristics of the orbit. The constant parameters ΔV_{T_0}, ΔV_{N_0}, D^*, and W in the performance index were chosen so that the one-dimensional search routine would converge in a reasonable number of iterations, which limited the number of orbit integrations required. The values selected were $\Delta V_{T_0} = \Delta V_{N_0} = 0.1$, $D^* = 100.0$, and $W = 100.0$.

Two cases were investigated to demonstrate the effectiveness of this maneuver strategy. Case 1 evaluated the ability of the maneuver strategy to maintain the satellite in the 125-m tube in the presence of the dominant perturbations, atmospheric drag, and luni–solar gravity, for one eight-day repeat cycle. Case 2 examined the viability of the maneuver strategy over four repeat cycles, or 32 days, in the presence of a full force model that additionally included solid Earth and ocean tides and radiation pressure. This longer interval was considered to identify trends in the longer-term behavior of the orbit and to assess the effectiveness of the maneuver strategy in addressing them.

Results of Fixed Interval Targeting

Because the satellite was expected to violate the tube in approximately 0.88 day, under the influence of drag alone, a maneuver at the initial epoch and a maneuver interval of approximately one day, or 15.5 orbits, were chosen for case 1. The calculated maneuvers are summarized in Table 4. Figure 5 shows that the maneuvers were able to maintain the satellite within the tube for eight days in the presence of both drag and luni–solar gravity. The alternating bands denote the interval between maneuvers. The eight maneuvers required a total ΔV of 131.072 mm/s.

In case 2, to examine the longer-term behavior of the orbit, the maneuver strategy was applied over four repeat cycles, nearly 32 days, using the more complete force model. As with case 1, a maneuver at the initial epoch and a nominal maneuver interval of 15.5 orbits were chosen. Subsequently, 18 maneuvers with tangential and normal components were calculated using the performance index G_1, and they are summarized in Table 5. However, subsequently it became

Table 4 Maneuver summary, case 1: drag and luni–solar models

Maneuver	Maneuver interval, s	ΔV_T, mm/s	ΔV_N, mm/s	Total ΔV
1	91,060.0	3.221	−0.255	3.476
2	91,060.0	22.755	2.616	25.371
3	91,060.0	11.611	−0.996	12.607
4	91,060.0	20.444	−1.647	22.091
5	91,060.0	16.771	−1.647	18.418
6	79,340.0	13.627	1.400	15.027
7	79,340.0	20.069	−2.269	22.338
8	73,460.0	10.418	1.326	11.744
Total	687,440.0	118.916	12.156	131.072

Table 5 Maneuver summary, case 2: full force models

Maneuver	Maneuver interval, s	ΔV_R, mm/s	ΔV_T, mm/s	ΔV_N, mm/s	Total ΔV
1	91,070.0	0.00	1.931	−0.151	2.082
2	91,070.0	0.00	23.473	2.635	26.108
3	91,070.0	0.00	15.220	−1.442	16.662
4	91,070.0	0.00	13.923	1.170	15.093
5	91,060.0	0.00	20.944	−2.234	23.178
6	91,060.0	0.00	15.168	1.434	16.602
7	91,060.0	0.00	16.309	−1.491	17.800
8	91,060.0	0.00	20.932	2.408	23.340
9	91,060.0	0.00	18.140	−8.304	26.444
10	91,060.0	0.00	16.025	24.467	40.492
11	91,060.0	0.00	16.572	−21.663	38.235
12	91,060.0	0.00	17.102	10.647	27.749
13	91,060.0	0.00	19.361	−2.076	21.437
14	91,060.0	0.00	17.438	1.437	18.875
15	91,070.0	0.00	21.216	2.037	23.253
16	91,070.0	0.00	8.352	−0.940	9.292
17	91,080.0	0.00	26.298	3.476	29.774
18	91,080.0	0.00	20.899	2.339	23.238
19	91,060.0	90.653	21.550	0.000	112.203
20	91,060.0	0.00	5.689	144.153	149.842
21	91,060.0	0.00	21.012	−2.396	23.408
22	91,060.0	0.00	19.714	4.932	24.646
23	91,060.0	0.00	17.294	−2.367	19.661
24	91,070.0	0.00	20.211	7.187	27.398
25	91,070.0	0.00	27.775	−3.244	31.019
26	91,080.0	0.00	3.022	0.167	3.189
27	91,080.0	0.00	27.620	7.811	35.431
28	91,080.0	0.00	18.854	−9.599	28.453
29	91,060.0	0.00	19.759	6.260	26.019
30	91,060.0	0.00	18.865	2.483	21.348
31	17,610.0	0.00	7.940	0.448	8.388
Total	2,749,590.0	90.653	538.608	281.398	910.659

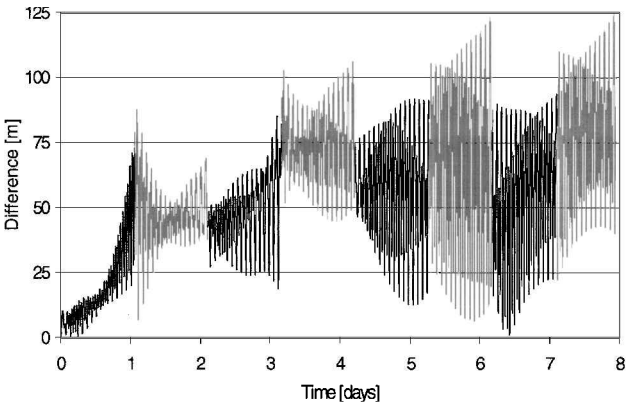

Fig. 5 Deviation from reference; case 1.

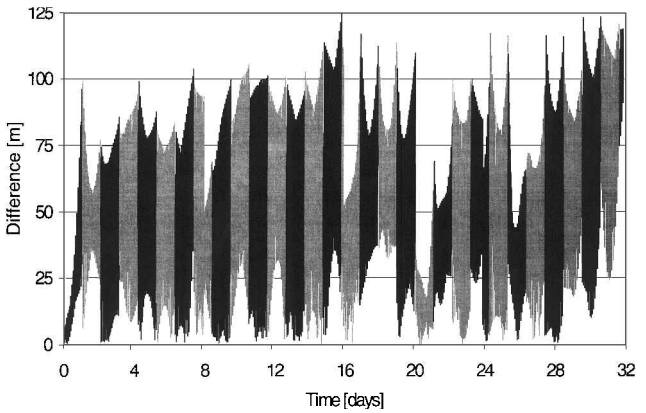

Fig. 6 Deviation from reference; case 2.

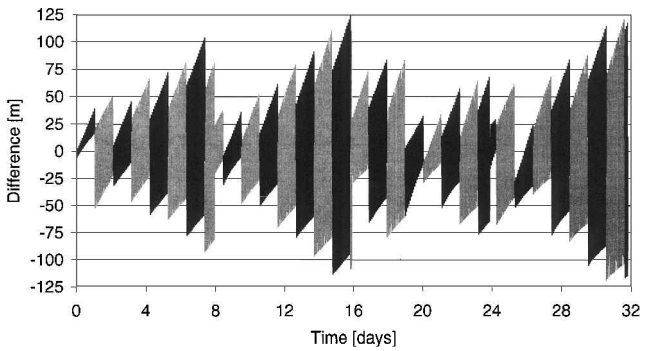

Fig. 7 Radial difference from reference; case 2.

necessary to reduce the spacing between maneuvers drastically to maintain the tube. It can be seen from Fig. 6, that by maneuver 18, the satellite no longer passes near the reference at the center of the tube, that is, the deviations no longer approach zero at any time. It was decided, at this point, to apply a set of corrective maneuvers to bring the satellite closer to the reference.

Figure 7 shows the radial deviation of the orbit from the reference. It can be seen that, despite the reductions in radial deviation due to the nominal maneuvers and the discontinuity in the reference itself, the radial deviation steadily increases with time. To reduce this accumulated radial deviation, a maneuver with components in the tangential and radial directions was applied. The magnitude of this maneuver was calculated by minimizing the following performance index:

$$G_2(\Delta V_T, \Delta V_R; t_m) = \frac{1}{W} \int D \, \mathrm{d}t \tag{3}$$

This performance index corresponds essentially to the area under the curve in Fig. 6. The integral was calculated using a rectangular approximation and a value of $W = 100{,}000.0$.

Because no limit was placed on the magnitude of this maneuver, its radial component of 90.653 mm/s is several times larger than the earlier calculated maneuvers. This maneuver was very effective in reducing the radial deviation of the orbit from the reference. Figure 8 indicates that the satellite deviates greatly in both the radial and cross-track directions following maneuver 18, but Fig. 9 shows that the radial deviation is significantly reduced after maneuver 19.

To reduce the large cross-track deviation that is still present after maneuver 19, a maneuver with tangential and normal components was calculated using a performance index of the same form as in Eq. (3):

$$G_3(\Delta V_T, \Delta V_N; t_m) = \frac{1}{W} \int D \, \mathrm{d}t \tag{4}$$

Maneuver 20, calculated from this performance index, has a very large normal component, 144.153 mm/s. Figure 10 shows that the

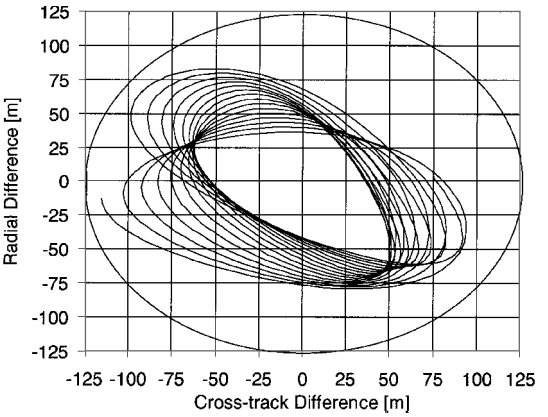

Fig. 8 Maneuver 18.

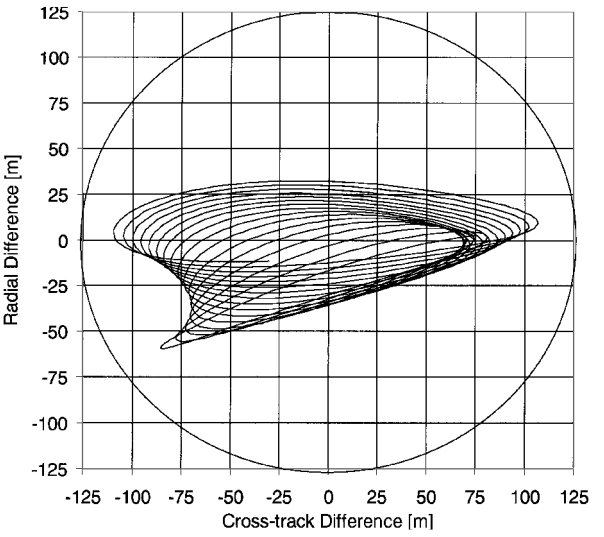

Fig. 9 Maneuver 19.

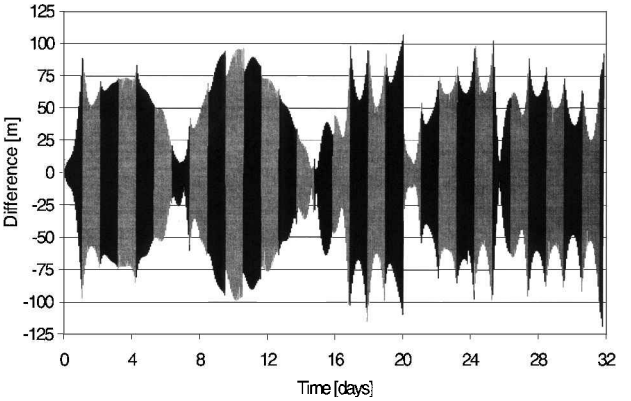

Fig. 10 Cross-track difference from reference; case 2.

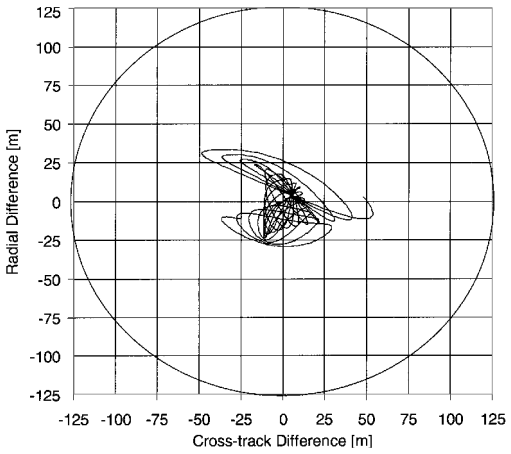

Fig. 11 Maneuver 20.

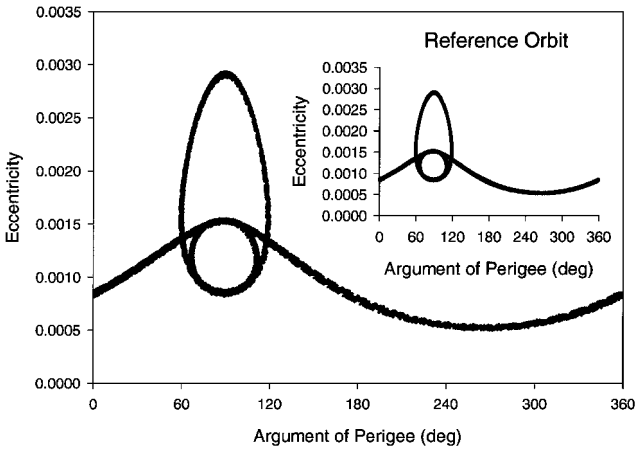

Fig. 12 Frozen orbit characteristics of maneuvered orbit.

cross-track deviation has been significantly reduced. After the application of these two maneuvers, the satellite again passes very near the center of the tube, as shown in Fig. 11.

The remainder of the maneuvers summarized in Table 5 were calculated using the original performance index. When this combination of nominal and corrective maneuvers are used, the satellite can be maintained within 125-m of the reference for four complete repeat cycles, nearly 32 days.

Figure 12 shows the eccentricity vs argument of perigee for the maneuvered and the reference orbits. It indicates that the frozen orbit characteristics were preserved for the maneuvered orbit over the four repeat cycles.

Comments on Maneuver Strategy

The first of the two cases examined demonstrated the ability of a fixed time interval maneuver strategy to maintain an orbit perturbed by drag and luni–solar gravity within a 125-m tube around a reference for a period of eight days. The second case, which included a full force perturbation model, revealed that, after 18 maneuvers, the deviation from the reference in both the radial and cross-track directions had accumulated significantly. Reduction of the accumulated radial deviation required application of a maneuver with a large radial component. Reduction of the accumulated cross-track deviation required application of a maneuver with a large normal component.

Over the course of the 32-day period studied, one radial and one cross-track corrective maneuver, totaling 234.806 mm/s, were required. Once these corrective maneuvers were applied, the fixed interval targeting strategy was able to maintain the orbit within the tube until the end of four repeat cycles. On average, approximately 21 mm/s of ΔV were applied per day, not including the maneuvers employed to remove the accumulated biases.

The results of this study indicate that it should be possible to maintain a satellite within a tube orbit for its mission lifetime. However, before a long-term maneuver strategy can be selected, several areas require further investigation.

This study used two forms of the performance index being minimized. The first minimized the ΔV applied, and the second minimized the deviation from the center of the tube. It should be determined which version of the performance index is more effective in maintaining the satellite within the tube. Further consideration should also be given to the values of the fixed parameters used.

A maneuver interval of 15.5 orbits was chosen for this study. A longer or shorter interval may improve the ability of the maneuver strategy to maintain the orbit. All of the maneuvers in this study were applied near the equator at either the ascending or descending node. Applying the maneuvers at some other location may improve their performance or eliminate the need for maneuvers with a radial component.

Maneuvers calculated in this study were limited to having components in two directions. Because it was necessary to apply a larger maneuver with a radial component, it would be worthwhile to examine a strategy that includes maneuvers that have components in three directions. If it is found that maneuvers to remove biases are necessary, the optimum spacing of these maneuvers should be determined.

Once a maneuver strategy and spacing have been selected, the long-term ability to maintain the orbit for a variety of drag and luni–solar conditions should be investigated. Orbit determination, satellite pointing, and maneuver execution errors will all impact the maneuver strategy, and their effects should be studied. If an effective maneuver strategy can be found, it could be automated for real-time operation of a satellite.

Conclusions

The LightSAR mission requires that the satellite orbit be maintained within a 125-m tube surrounding a reference orbit. By the use of the techniques developed by Lim and Schutz,[1] an eight-day, 117-revolution reference orbit was designed that is nearly periodic in the presence of the geopotential modeled through degree and order 70. It was found that the reference orbit repeated to within 7.5 cm in the horizontal direction and 16 m in the radial direction.

The effects of various perturbations were examined, including a 70×70 Earth gravity field, luni–solar gravity, ocean and solid Earth tides, atmospheric drag, and radiation pressure. For this study it was assumed that the area-to-mass ratio was 0.0133 m^2/kg, the solar flux $F_{10.7}$ was 200.0, and the geomagnetic index K_p was 2.0. The effects of each perturbation were investigated over a repeat cycle to determine the nature of the resulting deviations from the reference orbit. Atmospheric drag and luni–solar gravity were found to be the dominant perturbations that produced violation of the tube constraint. Neither Earth gravity model errors nor solar radiation pressure alone caused the satellite to violate the tube constraint during this interval.

A maneuver strategy that applied nominal maneuvers in the tangential and normal directions at fixed intervals was investigated. This strategy was found to be effective in maintaining the satellite within the required tube for one repeat cycle. Maintaining the satellite within the tube for longer periods of time required the application of larger corrective maneuvers in both the radial and normal directions to keep the satellite near the reference orbit. With the application of two corrective maneuvers it was possible to keep the satellite within 125-m of the reference orbit for 32 days.

This study indicates that it should be feasible to maintain a satellite within a 125-m-radius tube about a reference orbit. Several areas require further study before a long-term maneuver strategy can be selected. The optimum spacing and location of the maneuvers, as well as the form of the performance index used, should be investigated. A strategy using maneuvers with three ΔV components should be examined to determine if the corrective maneuvers applied in this study can be eliminated. Finally, the long-term behavior of the maneuver strategy should be studied under a variety of drag and luni–solar conditions.

Acknowledgments

Spectrum Astro under a study contract with the NASA Jet Propulsion Laboratory supported this research. Special thanks to the

referees, whose comments helped to improve the quality of this paper.

References

[1]Lim, S., and Schutz, B. E., "Orbit Maintenance and Maneuver Design for the EOS Laser Altimeter Satellite," American Astronautical Society, AAS Paper 95-220, Feb. 1995.

[2]Bhat, R. S., Frauenholz, R. B., and Cannell, P. E., "TOPEX/Poseidon Orbit Maintenance Maneuver Design," American Astronautical Society, AAS Paper 89-400, Aug. 1989.

[3]Tapley, B. D., Watkins, M. M., Ries, J. C., Davis, G. W., Eanes, R. J., Poole, S. R., Rim, H. J., Schutz, B. E., Shum, C. K., Nerem, R. S., Lerch, F. J., Marshall, J. A., Klosko, S. M., Pavlis, N. K., and Williamson, R. G., "The Joint Gravity Model 3," *Journal of Geophysical Research*, Vol. 101, No. B12, 1996, pp. 28,029–28,049.

[4]Kaula, W. M., *Theory of Satellite Geodesy*, Blaisdell, Waltham, MA, 1966, Chap. 4.

[5]Lemoine, F. G., Smith, D. E., Kunz, L., Smith, R., Pavlis, E. C., Pavlis, N. K., Klosko, S. M., Chinn, D. S., Torrence, M. H., Williamson, R. G., Cox, C. M., Rachlin, K. E., Wang, Y. M., Kenyon, S. C., Salman, R., Trimmer, R., Rapp, R. H., and Nerem, R. S., "The Development of the NASA GSFC and NIMA Joint Geopotential Model," *Gravity, Geoid, and Marine Geodesy*, Vol. 117, edited by J. Segawa, H. Fujimoto, and S. Okuba, Springer-Verlag, Berlin, 1997, pp. 461–469.

[6]Eanes, R. J., and Bettadpur, S., "The CSR 3.0 Global Ocean Tide Model Diurnal and Semi-Diurnal Ocean Tides from TOPEX/POSEIDON Altimetry," Center for Space Research CSR TM-95-06, Univ. of Texas, Austin, TX, 1995.

[7]Barlier, F., Berger, C., Falin, J. L., Kockarts, G., and Thuiller, G., "A Thermospheric Model Based on Satellite Drag Data," *Annales de Geophysique*, Vol. 34, No. 1, 1978, pp. 9–24.

[8]Synnes, D. C., "Precision Control of Frozen, Exact Repeat Orbits," American Astronautical Society, AAS Paper 93-726, Aug. 1993.

[9]Rim, H. J., Schutz, B. E., Webb, C. E., Demarest, P., and Herman, A., "Orbit Maintenance and Characteristics of a SAR Satellite," AIAA Paper 98-4394, Aug. 1998.

[10]Huang, H. Y., "Unified Approach to Quadratically Convergent Algorithms for Function Minimization," *Journal of Optimization Theory and Applications*, Vol. 5, No. 6, 1970, pp. 405–423.

F. H. Lutze Jr.
Associate Editor